Iranian Journal of Geophysics, Vol 19 No 3, 2025, Page 25–46 (Research Article)
DOI: 10.30499/ijg.2024.436293.1569

The Siberian high: changes in strength and its relationship with the Mediterranean cyclones from 1970 to 2020

Saeid Karbasi[1], Farhang Ahmadi-Givi [2*]and Alireza Mohebalhojeh [3]

[1] *M.Sc. Student, Institute of Geophysics, University of Tehran, Tehran, Iran*
[2] *Associate Professor, Space Physics Department, Institute of Geophysics, University of Tehran, Tehran, Iran*
[3] *Professor, Space Physics Department, Institute of Geophysics, University of Tehran, Tehran, Iran*

(Received: 21 January 2024, Accepted: 11 May 2024)

Abstract

As a large semi-permanent pressure system, the Siberian High (SH) has the potential to make impact on atmospheric circulation in vast areas of the Northern Hemisphere. This study aims to investigate the changes of the SH as well as the effects of SH on the characteristics of the Mediterranean cyclones in the period 1970–2020 using the Japanese 55-year Reanalysis (JRA-55) dataset. The method used is based on computing an index for the activity of the SH during winter season, analyzing the change points in the resulting time series, defining two subsets of years with high and low activity of the SH, and obtaining cumulative behavior of cyclones over four subareas of the Mediterranean.

Results establish that the activity of the SH has undergone a substantial weakening in the last two decades of the 20th century, followed by a resurgence of the SH since the early 21st century. The higher prevalence of cyclones during the subset of high SH activity years, particularly between 0˚ and 30˚ E longitudes, is found to be related to the changes in the winter mean tropospheric circulation, which can be interpreted as changes in the Northern Hemisphere stationary wave due to changes in the lower boundary induced by the SH. During the high-activity years, the main trough associated with the stationary wave over the Mediterranean undergoes a westward displacement by about 15˚ relative to the low-activity years. This is found to be a main factor in making the cyclonic activity different over the subareas considered.

Keywords: Extreme activity of Siberian high, resurgence, cyclonic activity, stationary wave

*Corresponding author: ahmadig@ut.ac.ir

1 Introduction

There are pressure systems that seem to persist for months or even seasons. A prominent example of such systems in the Northern Hemisphere (NH) during wintertime is the Siberian High (SH), which is a semi-permanent and quasi-stationary atmospheric pattern associated with the coldest and densest air mass in the NH (Lydolf, 1977; Ding and Krishnamurti, 1987, Ahrens and Henson, 2018). The lifetime of this shallow and cold-core anticyclone with the mean central sea level pressure of about 1030 hPa (Sahsamanglou et al., 1991; Takaya and Nakamura, 2005) starts in early October and lasts until late April. Maximum activity of the system occurs in boreal winter (i.e., December–February) and for this reason, most researches have used this time period in surveying the SH (e.g., Panagiotopoulos et al., 2005; Ahmadi-Hojat and Ahmadi-Givi, 2012; Tubi and Dayan, 2013; Zhao et al., 2018). The formation mechanism of the SH consists of a combination of dynamic and thermodynamic factors such as the mass convergence at middle and upper-level, and the vertical transfer of sensible and latent heat from the underlying surface (Ding and Krishnamurti, 1987; Ding, 1990).

An important issue that has been investigated extensively is the changes of SH during the recent history. A group of studies have shown that the SH has experienced a dramatic weakening in the last quarter of the 20th century, apparently associated with the global warming (e.g., Sahsamanglou et al., 1991; Panagiotopoulos et al., 2005; D'Arrigo et al., 2005; Tubi and Dayan, 2013), thereby resulting in the reduction of Eurasian snow cover (Jeong et al., 2011). At the same time, some studies also suggest that the SH has entered a period of considerable resurgence since the beginning of the 21st century which is also attributed to the global warming (e.g., Comiso et al., 2008; Jeong et al., 2011; Fei and Yong-Qi, 2015; Zhao et al., 2018). As discussed by Comiso et al. (2008) and Jeong et al. (2011), the significant melting of Arctic Sea ice may have affected moisture and energy fluxes in the Arctic and caused an increase in snowfall over the Eurasia, thereby leading to the resurgence of the SH. In this regard, Cohen et al. (2007) presented a dynamic model based on linkage between the strength of the SH and the amount of snow cover over the Eurasia. Given the uncertainties remaining on the time evolution of the SH during the last 50 years or so, this paper examines the likely shifts in the behavior of the SH using a particular "change point detection" method due to Rodionov (2004). Readers can consult with Aminikhanghahi and Cook (2017) for a survey of the change point detection methods.

Another aspect of interest has been the influence that the SH may exert on other atmospheric phenomena and teleconnection patterns. In this regard, Cohen et al. (2001) and Fei and Yong-Qi (2015) have shown that the SH accompanied by the Icelandic and Aleutian lows could substantially affect the formation of the atmospheric circulation patterns of various scales in the NH. Also, Rogers (1997) pointed out that the westward extension of the SH toward Europe, associated with southeasterly winds transporting air northwestward to the European region, influences the North Atlantic storm track. Amongst the regions that are expected to be impacted by the strength and geographical extension of the SH is the Mediterranean with its unique climatic conditions due to proximity of the Mediterranean Sea and the complex land topography (Trigo et al., 1999) and frequent cyclogenesis known since the early work by Petterssen (1956). Because of the existence of high mountains such as the Alps and Atlas, as well as sea surface temperature values higher than those of

the North Atlantic Ocean, the spatio–temporal distribution of cyclones in this region is highly complicated (Campins et al., 2010; Flocas et al., 2010; Almazroui et al., 2015, Lionello et al., 2016; Flaounas et al., 2022; Reale et al., 2022). A number of previous studies have examined some aspects of the SH impact on Mediterranean cyclones. Haggag and El-Badry (2013) and Dayan et al. (2015) have shown that the southward expansion of the SH increases the likelihood of developing extratropical cyclones and rainfall throughout the Mediterranean region. Almazroui and Awad (2016) stated that the path of eastern Mediterranean cyclones is related to the geographical extension of the SH. Moreover, the frequency of occurrence of cyclones in the Mediterranean region increases when the SH strengthens and stretches westward (Almazroui et al., 2017).

The first aim of this paper is to examine the evolution of SH over the time period from 1970 to 2020. To this end, the reanalysis dataset of JRA-55 has been used and compared with previous results obtained based on other datasets. Furthermore, two subsets of data related to years of high and low SH activity are based to compare the impact of SH during its strong and weak states. The second aim of this paper is to investigate the likely effects of the SH on the characteristics of the Mediterranean cyclones over the wintertime (December–February period or DJF for short) by comparing the characteristics during the extrema of SH. This is important as the Mediterranean cyclones are involved in shaping the weather and climate across a vast area over the Mediterranean, parts of North Africa and the Southwest Asia. As a novel feature, this is carried out for four regions encompassing the Mediterranean domain to cover the regional variations in the impact of SH.

The structure of the paper is as follows. The data and methodology are explained in Section 2. In Section 3, results for the changes in the SH regime during the study period are presented. Section 4 is devoted to the effects of the SH on the main characteristics of the Mediterranean cyclones such as the number, lifetime, intensity and path of cyclones in the extrema of SH activity. Finally, results are summarized and discussed together with main conclusions in Section 5.

2 Data and Methodology

The JRA-55 reanalysis dataset for winter season (DJF months) during which the SH is most active in its annual cycle, is used in this study. The JRA-55 consists of 6-hourly data with the horizontal resolution of 1.25˚ in both the zonal and meridional directions at 37 pressure levels. The reanalysis JRA-55 data for which modern data assimilation methods have been applied are available at ftp://ds.data.jma.go.jp (Kobayashi et al., 2015**)**. The study region that has been used to investigate the impacts of the SH on the Mediterranean cyclones is shown in Fig. 1. This region, extending from 20˚ to 50˚ N in latitude and 20˚ W to 50˚ E in longitude, is in the west, south and east directions, five degrees wider than the domain examined in Trigo et al. (1999) to accommodate the whole region under the influence of the Mediterranean storm track as defined by Hoskins and Hodges (2002). Rather similar choices can be found in Maheras et al. (2001) and Campins et al. (2010). The study region encompasses a widely varying area in terms of topography, land cover, land-sea contrast and geographical latitude. As our focus in this study is on integral or cumulative impacts of the SH, to cover the possible variations within the whole domain, the Mediterranean region is divided into four subareas named the northern (A), southern (B), eastern (C) and western (D) subareas. In this division, the subareas A and B together constitute the central area of Mediterranean whose

western boundary at 0˚ longitude and eastern boundary at 30˚ E follow no strict geographical meaning here. The divide between A and B in the central area is simply for making distinction between the north African region and the rest of the area. The rationale behind the subareas C and D is to examine the effects of the SH in the downstream and upstream of the Mediterranean storm track, respectively. In what follows, the methods used in the two parts of this study are presented.

a. The changes of the SH in the study period

Due to the thermal nature and shallow depth of the SH, it has mostly been investigated using the sea level pressure (SLP) (e.g., Gong and Ho, 2002; Panagiotopoulos et al., 2005; Jeong et al., 2011; Fei and Yong-Qi, 2015). Hence, in the first part, the monthly mean SLP from the JRA-55 dataset is used for analysis. To measure the amount of activity in each year, following Panagiotopoulos et al. (2005) an index called the Siberian high index (SHI) is defined as follows:

$$SHI_i = \frac{\overline{p_i} - \overline{\overline{p}}}{\sigma}, \qquad (1)$$

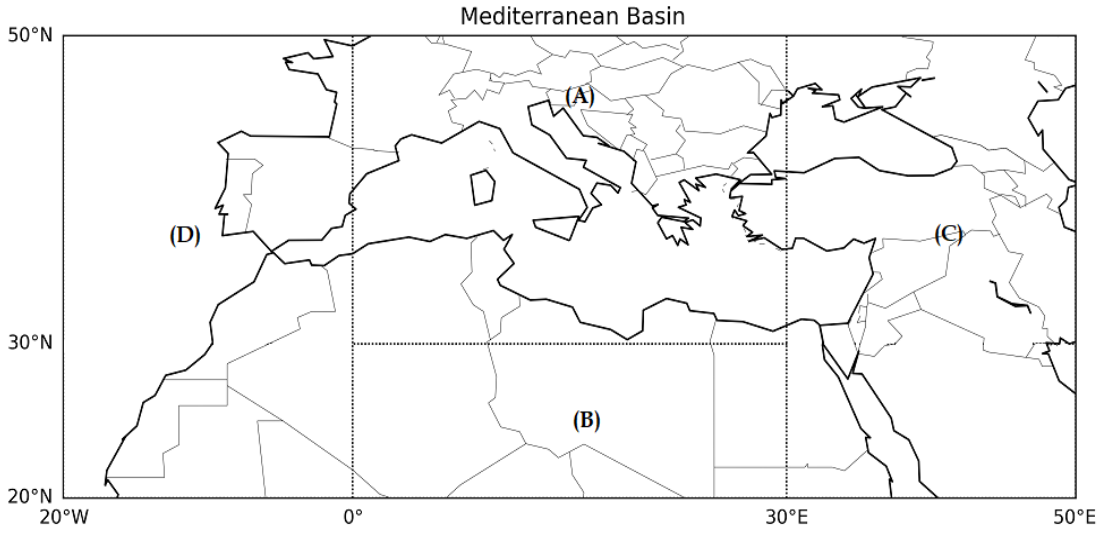

Figure 1. The study region including the Mediterranean basin. This region has been divided into four areas as: (A) northern (30˚-50˚ N and 0˚-30˚ E), (B) southern (20˚-30˚ N and 0˚-30˚ E), (C) eastern (20˚-50˚ N and 30˚-50˚ E), and (D) western (20˚-50˚ N and 0˚-20˚ W) for the detailed analysis.

where $\overline{p_i}$ is the average SLP over the main domain of the SH activity during each winter, $\overline{\overline{p}}$ is the corresponding climatological average over the entire study period, and σ denotes the standard deviation of the SLP. As in Panagiotopoulos et al. (2005) and Jeong et al. (2011), the main domain of the SH activity is taken to encompass 40˚ to 65˚ N and 80˚ to 120˚ E. Referring to relation (1), the SHI is nothing but a normalized SLP anomaly for each year. Due to the large fluctuations of the SHI, a purpose-built statistical method is needed to analyze its time series for detection of change points. For this, the so-called ‘‘climate regime shift’’ method of Rodionov (2004) is used here as a simple, yet powerful method to discover abrupt changes in the trends. Consisting of a seven-step algorithm, the method has found considerable application in climate change detection studies. Here, only an outline of the steps involved in the detection of change points is given and interested readers are referred to Rodionov (2004) for a complete description. The method starts by setting a

regime cut-off length l to calculate the difference *diff* between mean values of two subsequence regimes as:

$$diff = t\sqrt{2\sigma_l^2/l}, \quad (2)$$

where t is the value of t-distribution with $2l-2$ degrees of freedom and σ_l^2 is the average variance for the running l-year intervals in the time series. Then, based on $\overline{x}_{R1}$, the mean for regime R_1 over the initial l values of variable at hand, the levels that should be reached in the subsequent l years to qualify for a shift to regime R_2 are $\overline{x'}_{R2} = \overline{x'}_{R1} \pm diff$. So, for each new value starting with year $i = l+1$, if the value is greater than $\overline{x'}_{R1} + diff$ or less than $\overline{x'}_{R1} - diff$, then this year is considered as a possible start point j of the new regime R_2 and checked according to the steps involved in the rest of the algorithm.

The subsets of years with high and low SH activity are distinguished by index values of higher than 1 or less than -1 and referred to as SH^+ and SH^-, respectively. The two SH^+ and SH^- subsets determined based on DJF period (Table 1) will be used in presenting the results in Section 3. To give a broad perspective on the whole changes of the SH, the central core area of the SH, as defined in section 3.1, is also examined in the two subsets. The central core area is then used as a measure for the spatial extent of the SH. Moreover, by averaging SLP over the domain of the SH activity separately for each of the months during the extended winter (November through March), the month with maximum activity is determined. At the end of this part, the intraseasonal variability in activity of the SH is investigated by comparing the monthly mean SLP for the two subsets of extreme SH activity.

Table 1. The subsets of years with high and low SH activity (SH^+ and SH^-) during winter season in the 1970–2020 period. The number in front of each year refers to the Mediterranean cyclone frequency for that year.

Row	SH^+	SH^-
1	1977 (46)	1973 (19)
2	2005 (37)	1979 (45)
3	2006 (36)	1989 (17)
4	2012 (33)	1992 (24)
5	2016 (34)	1993 (17)
6	2018 (38)	1997 (30)
7	-	2007 (24)
8	-	2020 (26)

b. Effects of the SH on the characteristics of Mediterranean cyclones

In this part, the paper is focused on the two subsets of extreme years of SH activity. This makes it easier and more meaningful to compare the results and find out the relationship between the SH activity and the characteristics of the Mediterranean cyclones. To this end, the relevant characteristics of cyclones are determined using the cyclone tracking method proposed by Wernli and Schwierz (2006) by examining the 6-hourly maps of SLP in the Mediterranean region. Applying this method to the SLP maps, cyclones are identified with regions of closed contour

with values of less than 1009 hPa (Almazroui et al., 2017) that persist for at least 24 hours (Flocas et al., 2010; Flaounas et al., 2018) to retain only synoptically significant cyclones. The "lifetime" of a given cyclone is then simply the period of time during which the above criterion for that cyclone is held. The other characteristic that can be determined for a cyclone is the trajectory of its center from genesis stage to lysis stage, which is referred to here as the "path" of cyclone. The final characteristic to consider is the frequency of occurrence or simply the total number of cyclones per season for the two subsets of SH activity. It should be emphasized that the cyclones have been tracked and their characteristics have been recorded so long as they were in the defined area and the DJF period. This means that the cyclone statistics are carried out disregarding the origin of the cyclones.

3 Results

3.1 Changes of the SH in the study period

To start with, Fig. 2 shows the time series of the SHI for the JRA-55 dataset. What can be immediately seen is the presence of various degrees of fluctuation, from large to small, around the zero value which represents the climatological mean state. Dramatic changes are seen even within a short period of time, examples of which are the years 1977–1978, 2006–2007, and 2019–2020.

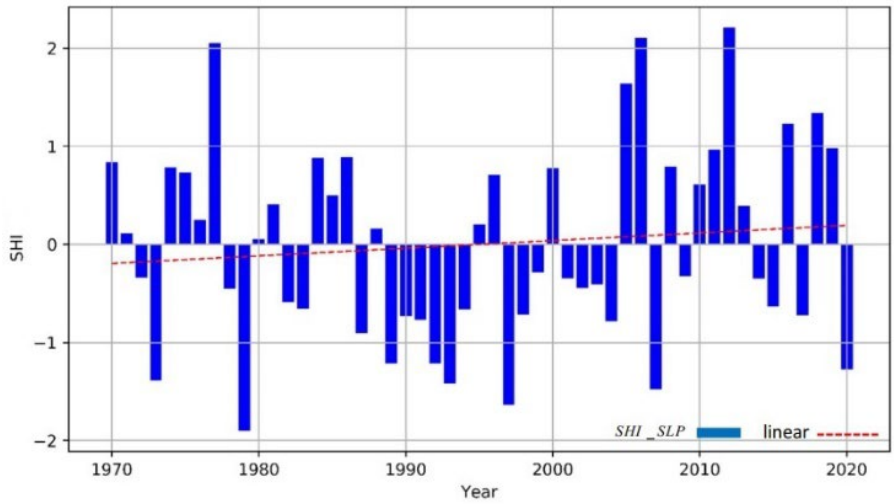

Figure 2. The time series of SHI for the winters (DJF) of the study period based on the SLP averaged over the area 40˚-65˚ N and 80˚-120˚ E using the JRA-55 dataset. The dashed line represents the linear regression for the whole time series.

For the whole period, the very low value of the coefficient of determination (R^2) means that the linear regression model fails to provide a reliable trend (see dashed line in Fig. 2). A question that arises in the analysis of such time series is the presence of rapid changes in the statistical behavior of the system. The ‘‘climate regime shift" method of Rodionov (2004) is used to answer the above question on changes in the SH activity. In the application of the method, the initial value for the cut-off length *l* in equation (2) is set to two years. Referring to Fig. 3, in this way, the time series diagram is divided into several smaller sections (red lines); for each section there is a well-defined mean value for SHI and thus the SH activity with jumps in mean value between the subsequent sections.

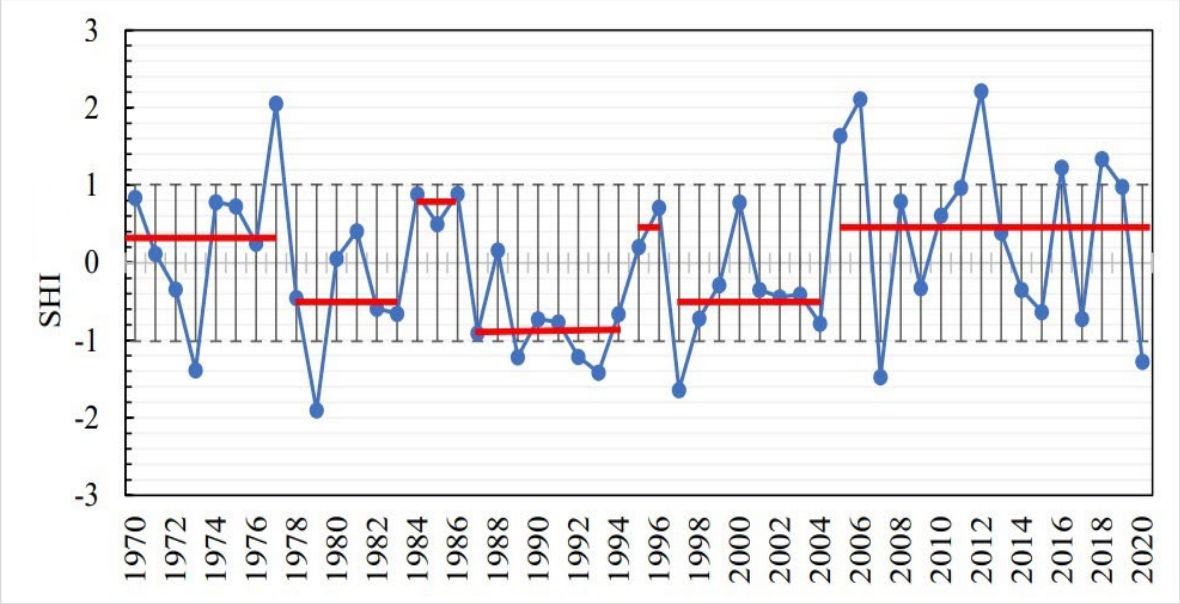

Figure 3. Similar to Fig. 2 but by applying the change point detection method discussed in the text. The blue line with circles represents the SHI values at different years over the study period, while the horizontal red lines indicate the time intervals for which the mean value is constant. The vertical bars denote the interval covered by minus and plus one standard deviation of the data.

Disregarding the two small periods of 1984–1986 and 1995–1996, one can distinguish a marked weakening of the SH during about 25 years from the late 1970s to 2004. The most severe weakening is related to the six-year period of 1989–1994. The method employed also points to a resurgence of the SH activity since 2005 to a mean value above that in early 1970s. In this period of resurgence, there are however large negative values in the SHI for 2007 and 2020 which seem to behave differently. It remains to be seen if the above resurgence would continue despite the weakening in 2020. Overall, these results on a period of weakening in the last quarter of the 20th century followed by a resurgence since the early 21st century are in agreement with the findings of the previous studies (e.g., Sahsamanglou et al., 1991; Panagiotopoulos et al., 2005; Jeong et al., 2011; Tubi and Dayan, 2013; Fei and Yong-Qi, 2015).

An interesting question is the extent to which the central core area and the spatial extent of the SH may vary between the two SH^+ and SH^- subsets (Table 1). Following Sahsamanglou et al. (1991) and Takaya and Nakamura (2005), the central core of the SH is considered as an area with the mean SLP equal to or greater than 1030 hPa. To shed light on the above question, the seasonal means of SLP in the SH^+ and SH^- subsets as well as the whole set of years are presented in Fig. 4. Comparing Figs. 4a and 4b (or Figs. 4d and 4e), one can see that the central core area of the SH in the SH^+ subset is larger than that of the SH^- subset. The SH^+ subset has higher zonal and meridional extensions (30˚-70˚ N, 60˚-130˚ E) than the SH^- subset (40˚-55˚ N, 80˚-115˚ E). With an extension of (40˚-60˚ N, 75˚-120˚ E), the central core of the SH in the whole set (Figs. 4c and 4f) is between the two extremum subsets of SH activity. Our results on the spatial extent of the SH in the long-term mean is consistent with the previous findings (e.g., Gong and Ho, 2002; Tubi and Dayan, 2013; Fei and Yong-Qi, 2015) that the central core of the SH covers the entire continent of Asia, from China to Turkey, and many parts of Russia associated with its extension to the Arctic.

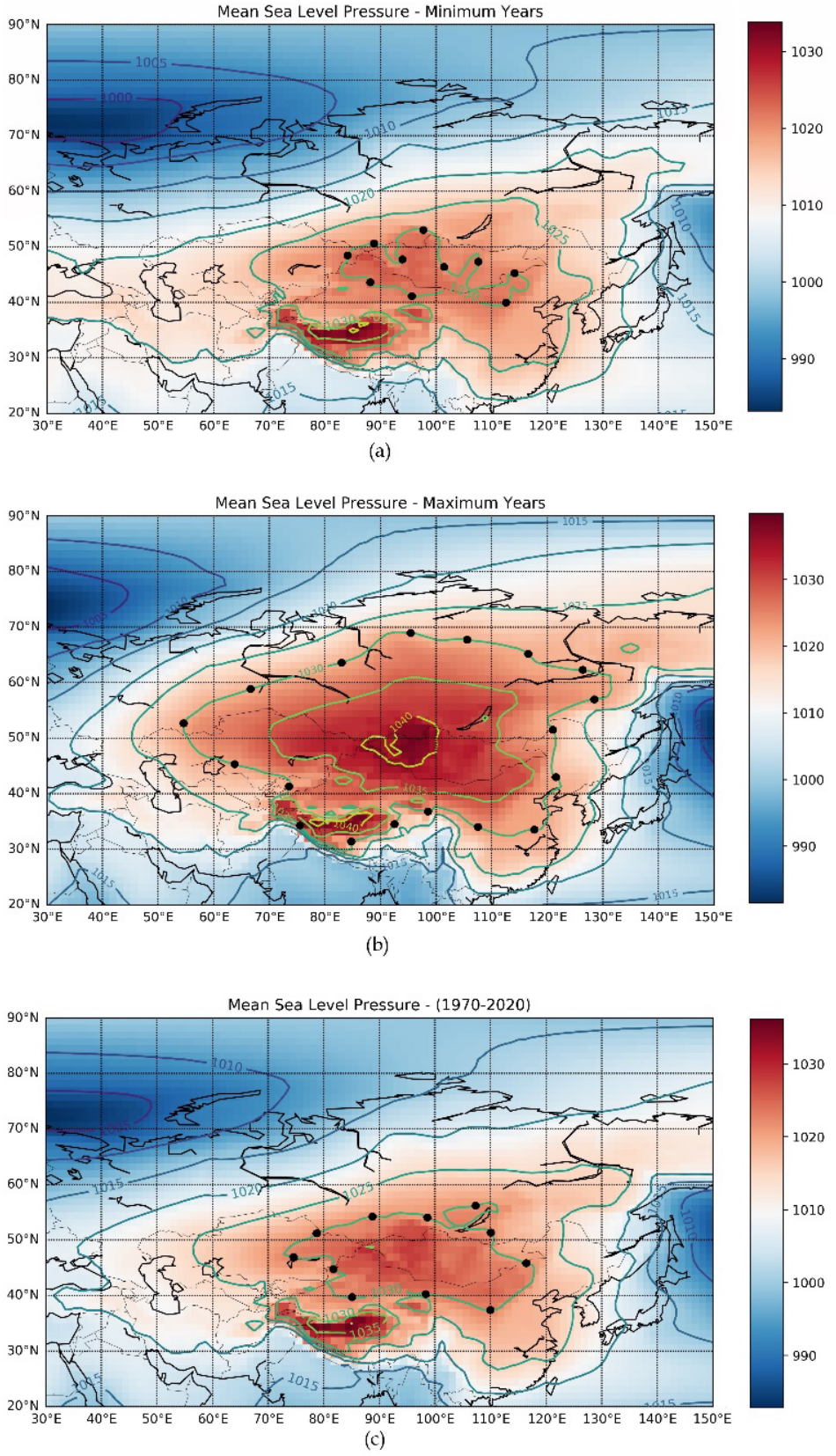

Figure 4. The distributions of the seasonal mean SLP (in hPa) including the central core of the SH, marked by black circles, for wintertime based on the JRA-55 dataset in: (a) the SH^- subset, (b) the SH^+ subset, and (c) the whole set of years.

For a grasp of intraseasonal variability, the monthly mean SLP averaged over the domain of the SH activity (40˚ to 65˚ N and 80˚ to 120˚ E) in the extended winter (November to March) is presented in Fig. 5a. Note that the domain chosen is the same as that used in the definition of the SH index in section 2a. The highest activity of the SH occurs in January. Similar results but only for the DJF are shown in Fig. 5b for the SH^+ and SH^- subsets. As can be seen, the intraseasonal variability in the two subsets is similar to that in the whole set of winter months, the only difference being the greater (lower) values in the SH^+ (SH^-) subset. This means that anomalous increase or decrease of the SH activity has no impact on the intraseasonal variability such that the SH strengthens in December, reaches its maximum activity in January, and subsequently weakens in February.

It is worth pointing out that the results presented in this section are in general agreement, in their common time period, with the results of Panagiotopoulos et al. (2005), Jeong et al. (2011), and Fei and Yong-Qi (2015) who used other datasets including those of the NCEP/NCAR (National Centers for Environmental Prediction/ National Center for Atmospheric Research) and the ERA40 and ERA-Interim of ECMWF.

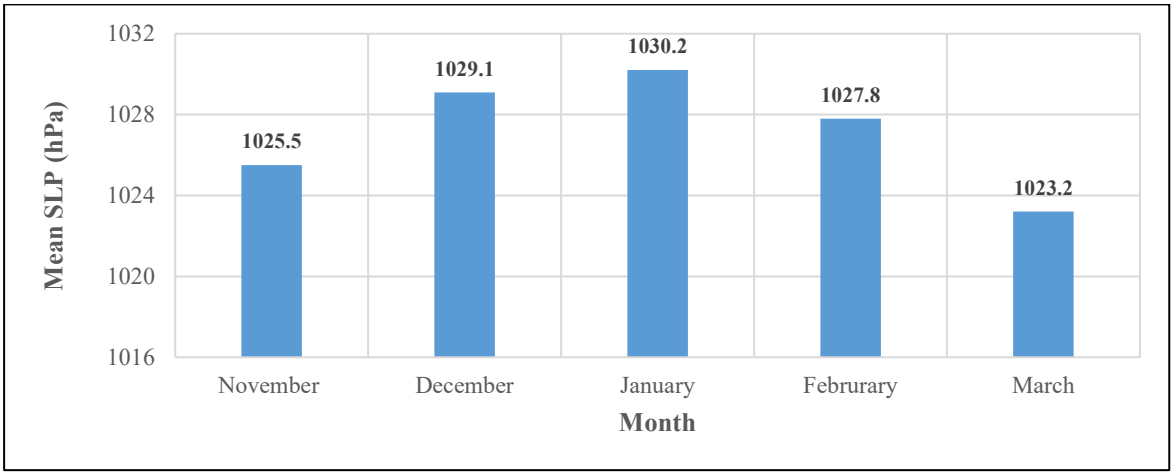

(a)

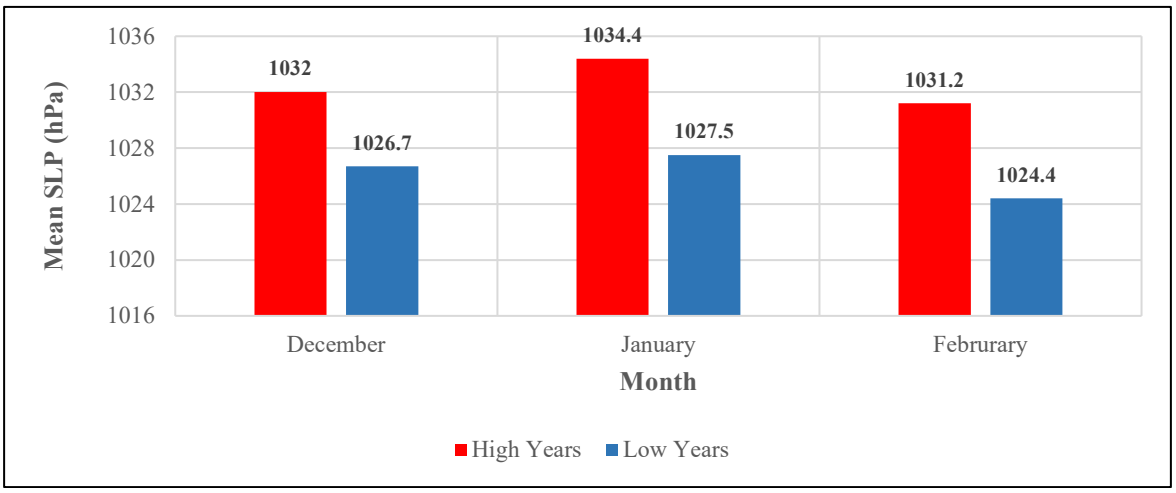

(b)

Figure 5. The monthly mean SLP (in hPa) averaged over the domain of SH activity for a) each month from November to March of the entire time period (1970–2020), and b) each month from December to February of the SH^+ and SH^- subsets using the JRA-55 dataset.

3.2 The associated climatological mean flow

To examine the changes in the background in which synoptic activity takes place over the Mediterranean and its surrounding, Fig. 6 presents the winter mean distributions of geopotential height for the selected pressure levels of 850, 500, and 300 hPa as well as temperature for the 850 hPa level and relative vorticity for the 500 and 300 hPa levels. The ridge of geopotential height associated with the SH at the 850 hPa level is of noticeably higher amplitude and displaced further to the west in the SH^+ subset (cf. Figs. 6a and 6d). The latter ridge is accompanied by a trough in its upstream over the west of Asia and Europe, which undergoes significant changes under the influence of the SH. In this regard, one can distinguish a difference between the Rossby wave structure north and south of 50˚ latitude at 850 hPa level. At midlatitudes north of about 50˚ latitude, the wave is tilted in the northwest–southeast direction over Europe at around 30˚ E and in the northeast–southwest direction at about 45˚ E. At the south of 50˚ latitude, while in the SH^+ subset, the dominant features are the presence of the subtropical high pressure and a trough line at about 20˚ E, in the SH^- subset, the dominant feature is a trough line slightly to the east of 30˚ E at the tip of the Red Sea. The higher strength of the high pressure over the north of Africa and Saudi Arabia in the SH^+ is consistent with the findings reported in Hasanean et al. (2013). Upstream of the domain of activity of the SH, the same north–south divide noted above is also seen at both the 500 and 300 hPa pressure levels. In the SH^+ (Figs. 6b and 6c), a mid-latitude non-tilted trough at about 30˚ E and a northeast–southwest tilted trough further to the west and to the south of 50˚ N are the dominant features. In the SH^- (Figs. 6e and 6f), however, one can see only a northeast–southwest tilted trough which is at about 20˚ to the east of its counterpart in the SH^+.

The approximately zonal band of significant positive values of relative vorticity at Figs. 6c and 6f at 30˚ N are related to the subtropical jet. The northeast–southwest tilted trough at the mid to upper troposphere may reflect the Rossby wave breaking and the associated southward wave-activity flux (Thorncroft et al., 1993). Depending on the position of the above-mentioned northeast–southwest tilted trough, the positive values of relative vorticity are stronger over the northwest of Africa in the SH^+ and over the tip of the Red Sea in the SH^-. It is worth noting here the statistically

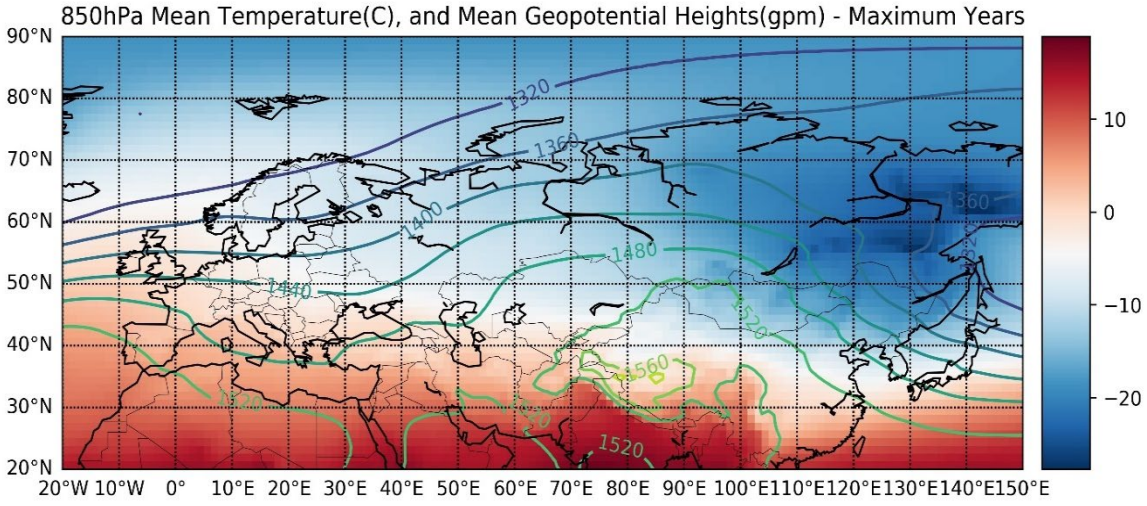

(a)

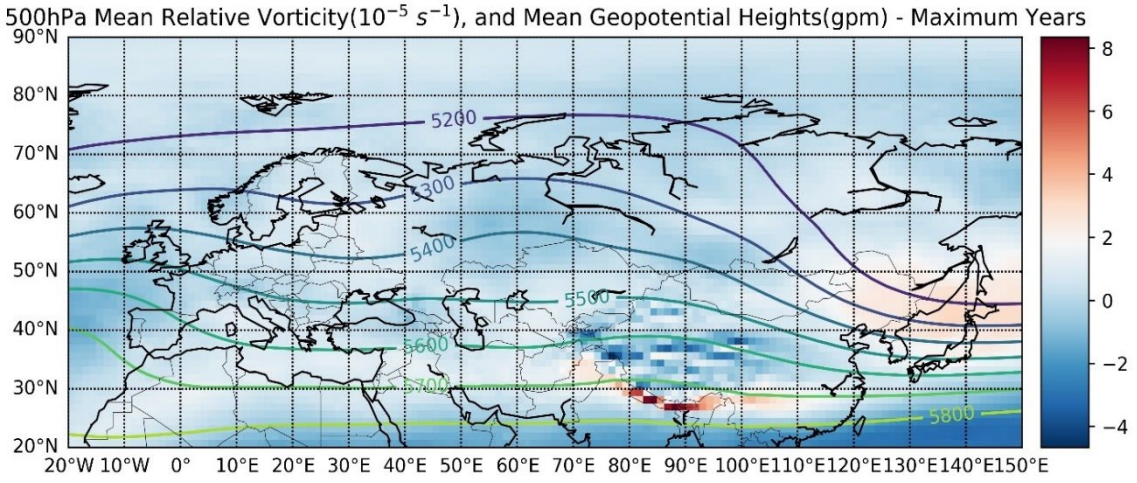
500hPa Mean Relative Vorticity(10^{-5} s^{-1}), and Mean Geopotential Heights(gpm) - Maximum Years
5200
5300
5400
5500
5600
5700
5800
90°N
80°N
70°N
60°N
50°N
40°N
30°N
20°N
20°W 10°W 0° 10°E 20°E 30°E 40°E 50°E 60°E 70°E 80°E 90°E 100°E110°E120°E130°E140°E150°E
8
6
4
2
0
−2
−4

(b)

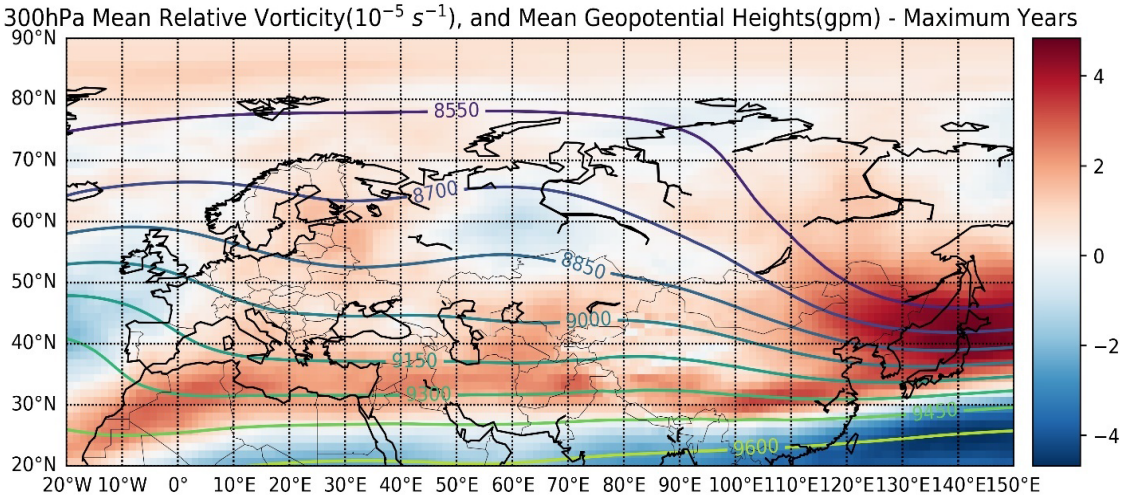
300hPa Mean Relative Vorticity(10^{-5} s^{-1}), and Mean Geopotential Heights(gpm) - Maximum Years
8550
8700
8850
9000
9150
9300
9450
9600
90°N
80°N
70°N
60°N
50°N
40°N
30°N
20°N
20°W 10°W 0° 10°E 20°E 30°E 40°E 50°E 60°E 70°E 80°E 90°E 100°E110°E120°E130°E140°E150°E
4
2
0
−2
−4

(c)

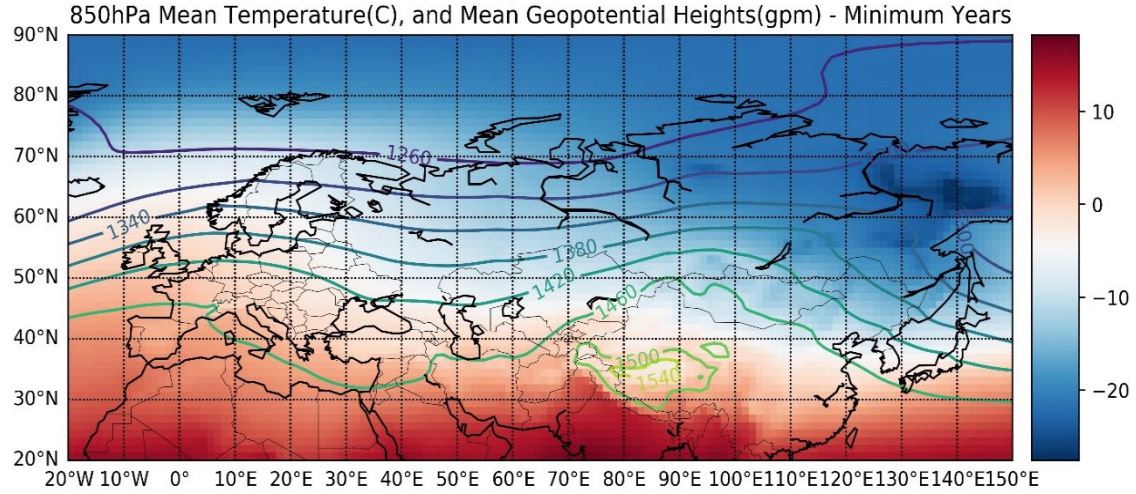
850hPa Mean Temperature(C), and Mean Geopotential Heights(gpm) - Minimum Years
1260
1340
1380
1420
1460
1500
1540
90°N
80°N
70°N
60°N
50°N
40°N
30°N
20°N
20°W 10°W 0° 10°E 20°E 30°E 40°E 50°E 60°E 70°E 80°E 90°E 100°E110°E120°E130°E140°E150°E
10
0
−10
−20

(d)

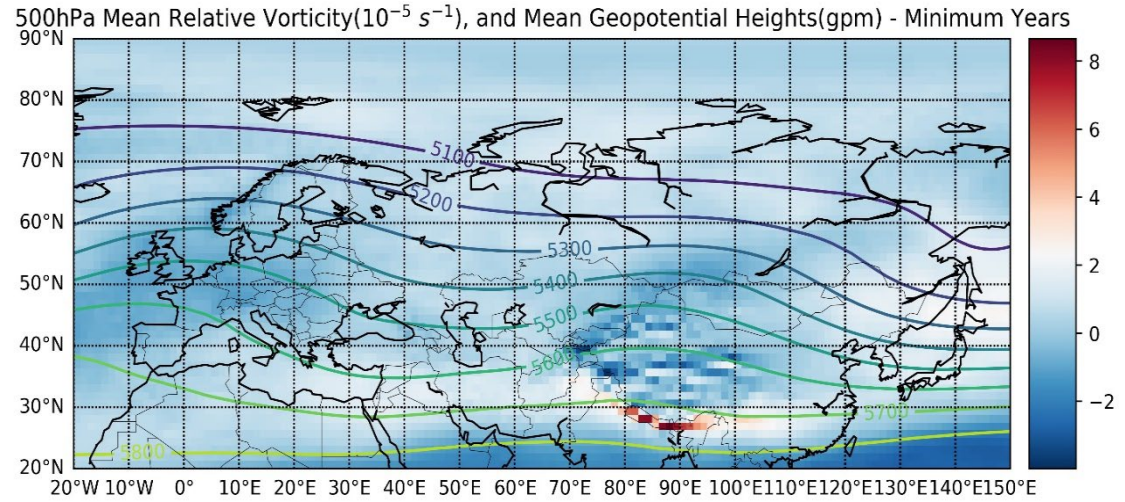

(e)

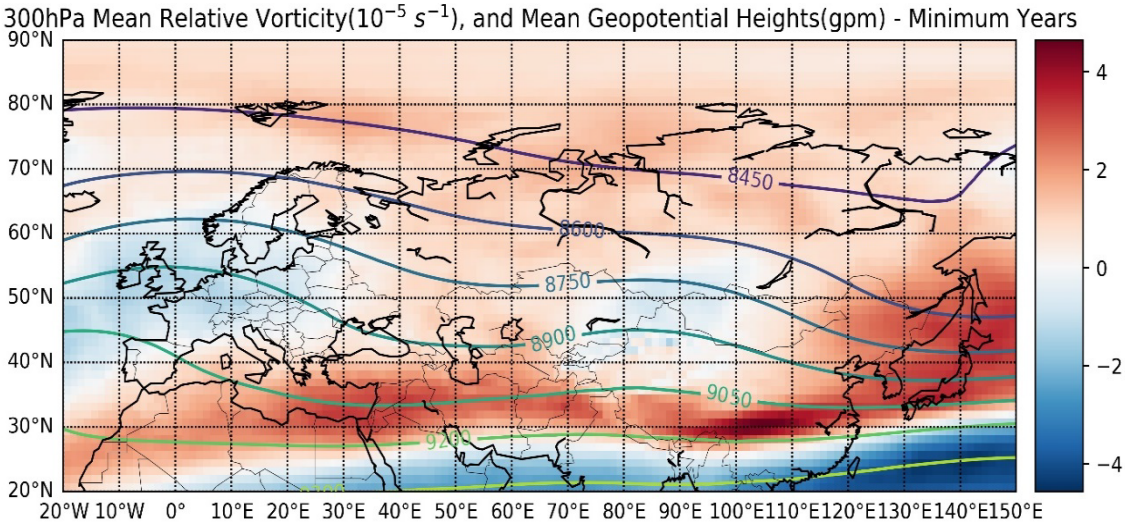

(f)

Figure 6. The distributions of the seasonal mean (a, d) 850-hPa geopotential height (contours) and temperature (shaded), (b, e) 500-hPa geopotential height (contours) and relative vorticity (shaded), and (c, f) 500-hPa geopotential height (contours) and relative vorticity (shaded) for (a–c) the SH^{+} subset and (d–f) the SH^{-} subset.

significant positive correlation of the SHI with the zonal wind at 200 hPa pressure level near to the tip of the Red Sea presented in Fig. 8b of Panagiotopoulos et al. (2005). The changes noted above throughout the troposphere are expected to have consequences on the cyclonic activity in the region.

To shed further light on the impact of Siberian high, for the geopotential height at 500 hPa pressure level, the difference field of high-activity years minus low-activity years, i.e. $SH^{+} - SH^{-}$, is shown in Fig. 7. The presence of the low over the north of Mediterranean is the main feature that proves useful in understanding the results in what follows for the Mediterranean cyclones.

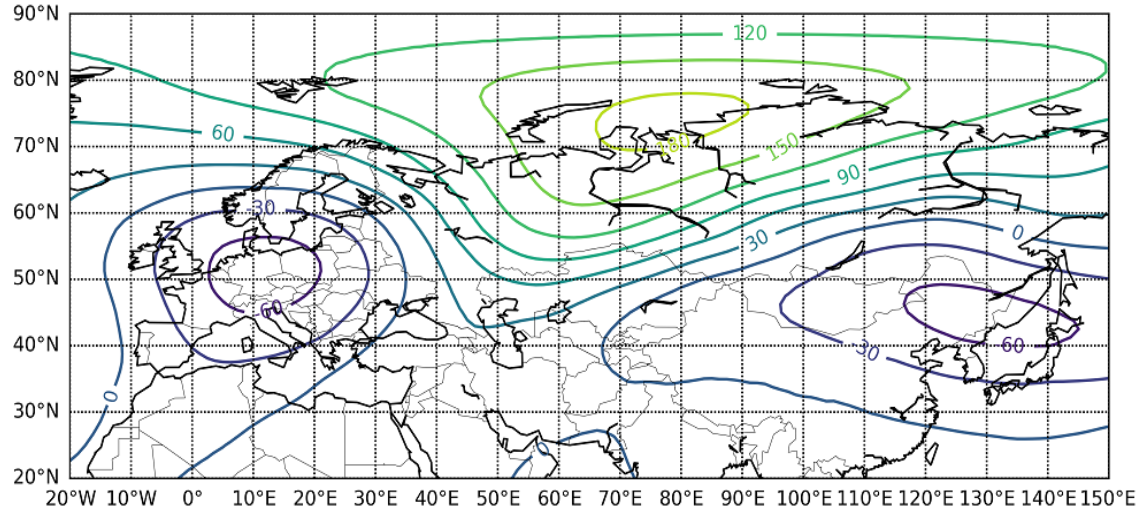

Figure 7. The seasonal mean 500-hPa geopotential height (contours in gpm) difference between the SH^+ and SH^- subsets.

3.3 Effects of the SH on the characteristics of Mediterranean cyclones

To begin with, the climatological mean frequency of occurrence of the Mediterranean cyclones coincident with the two SH^+ and SH^- subsets is compared. The average frequency of cyclones occurred in the SH^+ and SH^- are, respectively, 37.3 and 25.2 cyclone per year. This means that the average frequency of cyclones occurred in the SH^+ subset is about 67% greater than that in the SH^- subset. This difference is statistically significant at 0.01 level in a one-way ANOVA (analysis of variance) with the null hypothesis of equal means. Further, one can see a clear separation in terms of frequency of occurrence per each year between the two SH^+ and SH^- subsets (Table 1), if the anomalous year of 1979 in the SH^- with 45 Mediterranean cyclones is disregarded. The large number of cyclones in 1979 comes mainly from the contribution of the western subdomain of Mediterranean and is likely due to the large-scale circulation factors that are not controlled by the SH.

We now discuss the possible effects of the SH on the characteristics of the Mediterranean cyclones. As stated before, to cover the significant regional variation of cyclone characteristics in the Mediterranean (e.g., Trigo et al., 1999; Trigo et al., 2002; Campins et al., 2010; Almazroui et al., 2017), results are presented separately for each subarea of the region shown in Fig. 1. As a characteristic of motion, for each subarea, the cyclones that travel outside the subarea are grouped together and distinguished from those that are confined to their subarea. The former and the latter cyclones are of the travelling and confined types, respectively.

a. The northern subarea

The characteristics of cyclones in the northern subarea of the Mediterranean region coincident with the subsets of years with high and low SH activity are presented in Fig. 8. According to Fig. 8a, in this subarea, the seasonal mean number of cyclones in the SH^+ subset is about 68% higher than in the SH^- subset. As was the case for the entire Mediterranean region, the difference between SH^+ and SH^- is statistically significant at 0.01 level in a one-way ANOVA (analysis of variance) with the null hypothesis of equal means. The percentage of the most persistent cyclones of 96–120 hours duration is also noticeably greater in the SH^+ subset (see Fig. 8b). Moreover, it can be deduced from Fig. 8c that in the SH^+, a significant portion of cyclones formed in

the northern subarea of the Mediterranean region are of the confined type. The situation is reverse in the SH^-; a greater portion of cyclones are of the travelling type, often move to the east and northeast of the Mediterranean region.

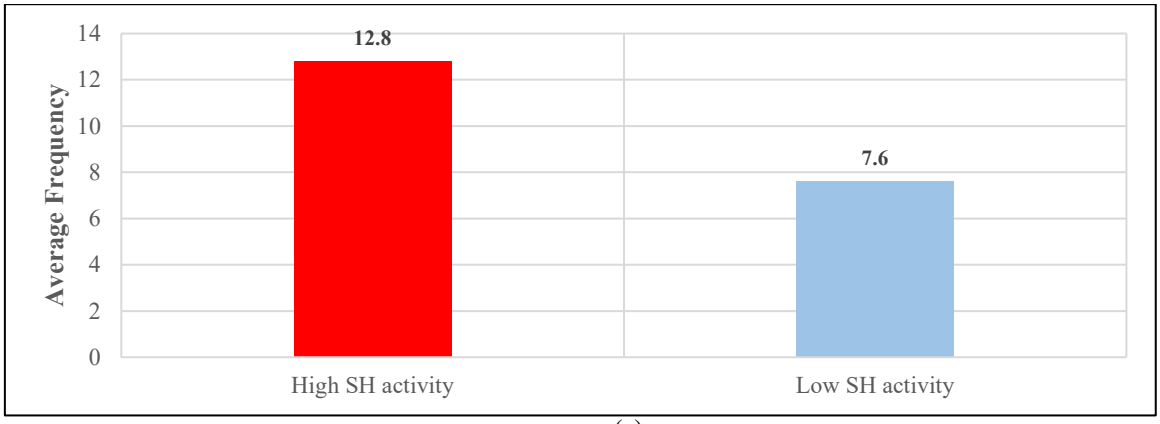

(a)

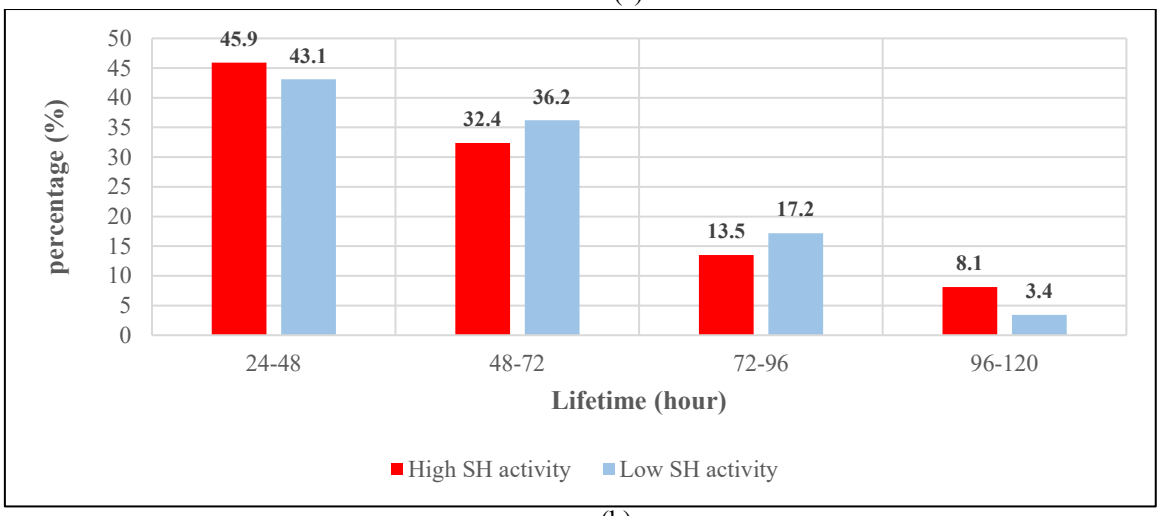

(b)

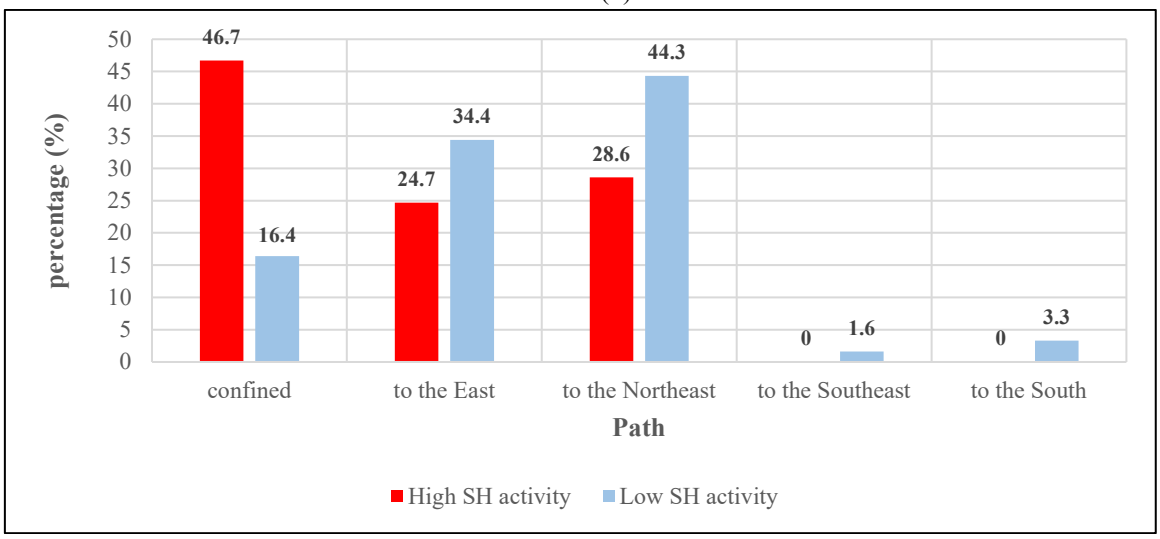

(c)

Figure 8. The characteristics of cyclones of the northern subarea of the Mediterranean region in the subsets of SH^+ (red bar) and SH^- (blue bar); a) average number of cyclones per year, b) lifetime, c) path.

As a whole, the main effects on the characteristics of cyclones in the northern subarea of the Mediterranean region can be identified as (i) a significant increase in cyclogenesis and (ii) the percentage of the confined type cyclones during high SH activity. To understand the first effect, one should note that the expansion of the SH toward Europe influences the North Atlantic and the Mediterranean storm tracks by displacing the main baroclinic zone to the south, enhancing baroclinicity in the Mediterranean, and altering the background static stability of the atmosphere (see related discussion in Ding, 1990; Rodwell et al., 1999; Trigo et al., 1999; Eshel et al., 2000; Nasr-Esfahany et al., 2011; Rezaeian et al., 2016). The changes induced in the baroclinicity and static stability are expected to lead to changes in the growth rate of the cyclones and thus their characteristics (Soldatenko and Tingwell, 2013). The higher percentage of the confined type cyclones can be related to the fact that the SH has also a barrier effect which inhibits the eastward movement of cyclones. This barrier effect is expected to increase during the high activity years of SH.

b. The southern subarea

Figure 9 illustrates the seasonal mean frequency of cyclones in the southern subarea of the Mediterranean region associated with the two SH^+ and SH^- subsets. Given that on average only one to two cyclones occur per winter, this subarea can be regarded as being rather inactive and therefore, no further discussion is made here on the SH impact.

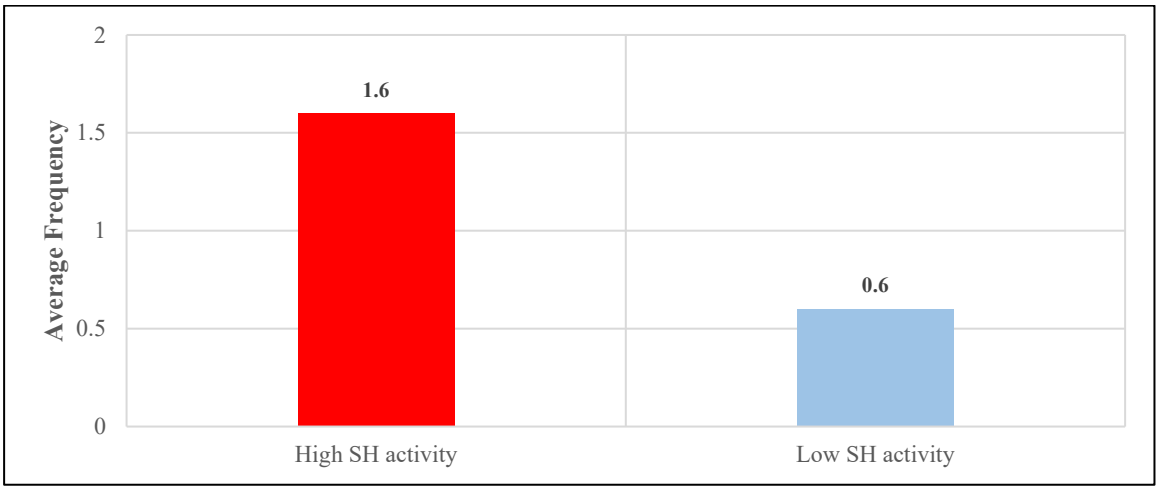

Figure 9. Similar to Fig. 8a but for the southern subarea of the Mediterranean region.

c. The eastern subarea

The characteristics of cyclones occurred in the eastern subarea of the Mediterranean region during the two subsets of SH activity is displayed in Fig. 10. As can be seen in Fig. 10a, the seasonal mean frequency of occurrence of cyclones is almost the same for the two SH^+ and SH^- subsets. Referring to Fig. 10b, the percentage of cyclones is greater in the SH^+ subset for the lifetimes of 24–48 hours, but the reverse is the case for the longer lifetimes of 48–72 hours. The characteristics of cyclones in terms of motion, that is, being of confined or travelling type, show much less variation between the two subsets (Fig. 10c) when compared to the northern subarea.

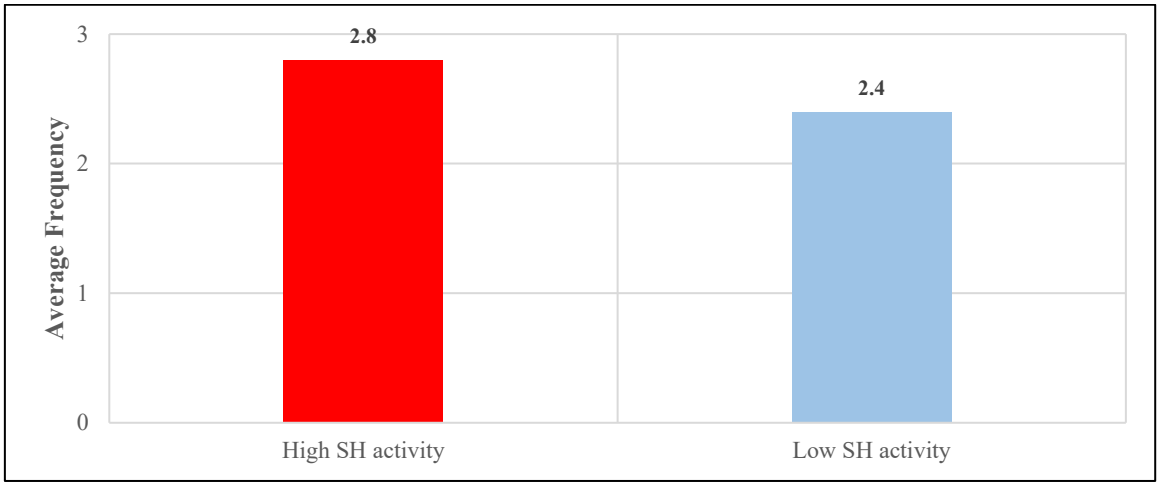

(a)

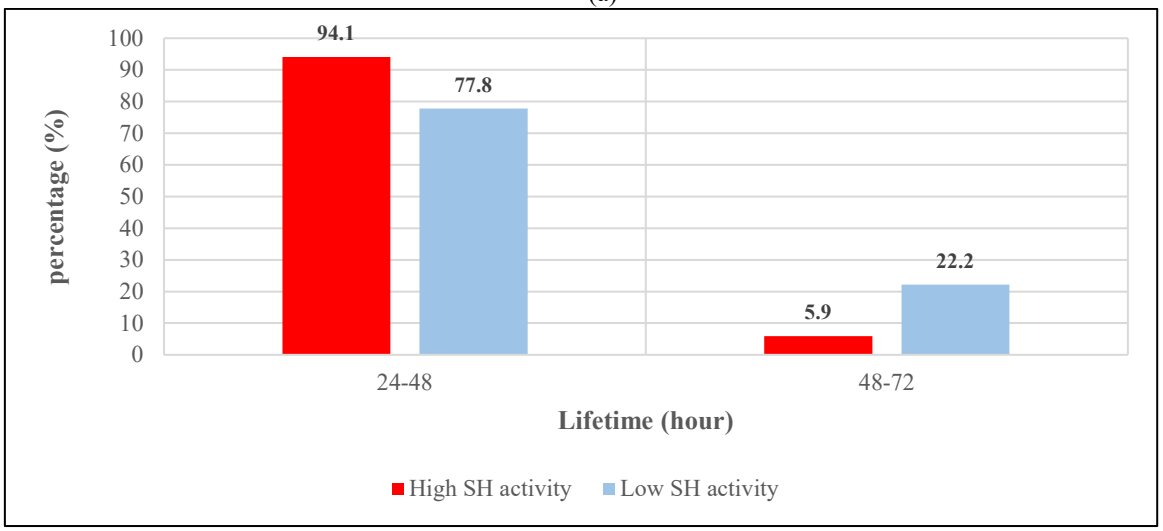

(b)

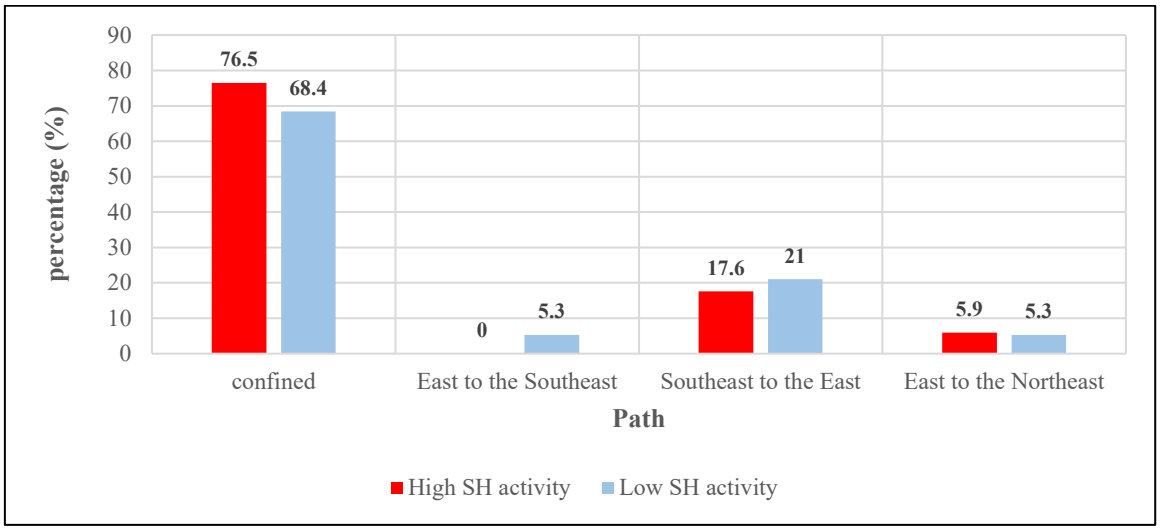

(c)

Figure 10. Similar to Fig. 8 but for the eastern subarea of the Mediterranean region.

Overall, in the eastern subarea, the characteristic that shows certain sensitivity to the SH activity is the lifetime of cyclones. The fact that the frequency of occurrence of cyclones remains much less sensitive to the SH activity is consistent with the dominance of upstream influence on cyclogenesis in this area, which takes place by the transmission of Rossby wave activity from the North Atlantic and Mediterranean storm tracks (see e.g., Eshel and Farrel, 2000; Eshel et al., 2000; Almazroui et al., 2015; Alizadeh et al., 2020).

d. The western subarea

In Fig. 11, the characteristics of cyclones in the western subarea of the Mediterranean are shown for the SH^+ and SH^- subsets. Referring to Fig. 11a, the winter mean frequency of cyclones in the SH^+ subset is only 8% higher than that in the SH^- subset, which constitutes the least relative increase in cyclogenesis over the subareas in the SH^+. For the relationship between the distribution of cyclone frequency in different lifetimes and the extrema of SH activity (Fig. 11b), it seems that the cyclones with a lifetime beyond 96 hours tend to occur in the SH^- subset more frequently. Based on Fig. 11c for the movement of cyclones, about 28% and 37% of cyclones can be classified as being of confined type in, respectively, the high- and low-activity years of the SH. Among the cyclones of travelling type, the most populated is that of the group moving from the west toward the north, followed by the group moving zonally toward the east with a percentage higher in the SH^- subset.

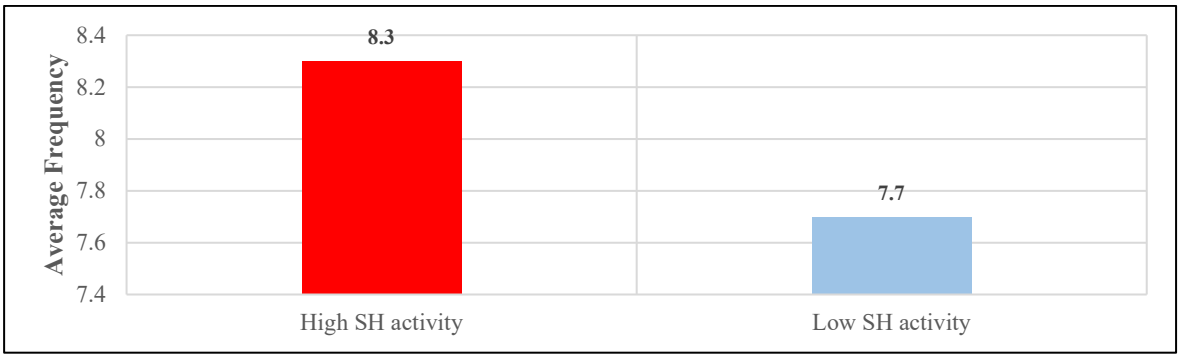

(a)

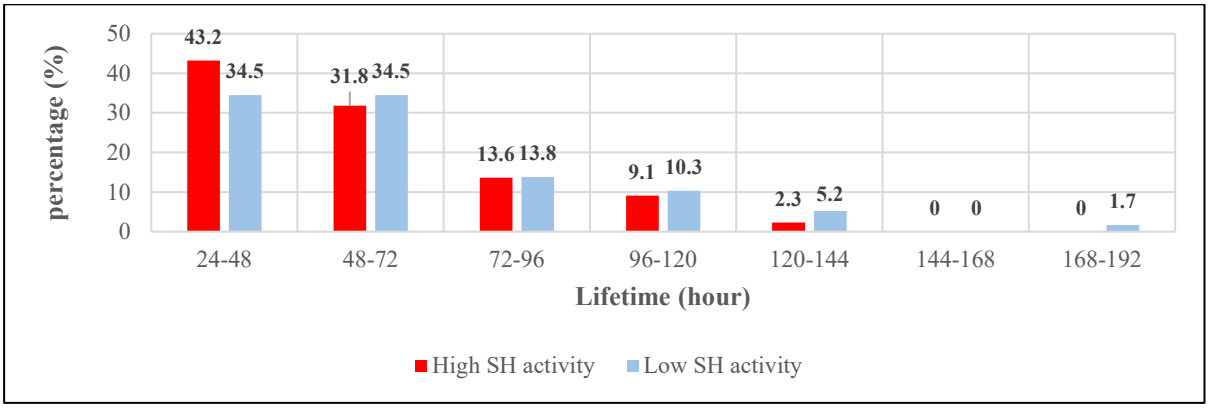

(b)

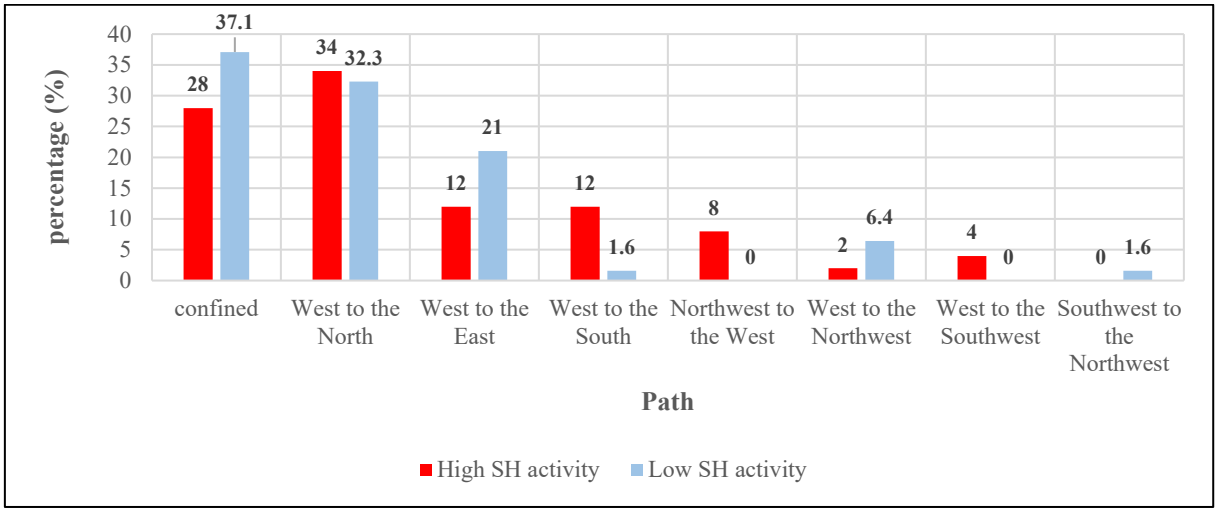

(c)

Figure 11. Similar to Fig. 8 but for the western subarea of the Mediterranean region.

4. Conclusion

This study aims to investigate the changes of the SH during the period of 1970–2020 and the likely effects of the SH on the characteristics of the Mediterranean cyclones using the reanalysis dataset of JRA-55. To this end, first an index similar to that of Panagiotopoulos et al., (2005) based on the mean SLP was applied to the winter months (DJF) when the SH is at its highest activity. An algorithm for change point detection, originally designed for detection of "climate regime shifts", was applied to the time series of the SH index to determine the regimes and change points of the SH. Then two subsets of years with extremely high and low SH activity, called respectively SH^{+} and SH^{-}, were identified for which the features of SH such as the central core area and its spatial extent were compared. Thereafter, the impacts of the SH on the characteristics of the Mediterranean cyclones were examined by comparing the cyclone statistics during the subsets of high- and low-activity SH. To obtain the cyclone statistics, use was made of the cyclone tracking method proposed by Wernli and Schwierz (2006). The focus was on the cumulative characteristics of cyclone activity over the four subareas defined in Fig. 1 for the Mediterranean domain and its surrounding that overall constitute the Mediterranean storm track. Application of the specific change point detection method established that in terms of the SH activity, the marked weakening during the last two decades of the 20th century, especially in the 1990s, was followed by a resurgence of the SH during the first two decades of the 21st century. An intraseasonal variability was found during which the SH activity peaks in January in the entire study period with no sensitivity to the amount of SH activity.

Theoretically, the changes observed in the characteristics of the Mediterranean cyclones associated with the two subsets of extreme SH activity, can be understood in terms of the effect of the SH on shaping the Northern Hemisphere winter stationary wave (for the relevant information see Wallace, 1983; Held et al., 2002) by the changes in the lower boundary thermal forcing. Compared to the subset of years with low SH activity, results pointed to a clear westward displacement of the main trough associated with the winter stationary wave upstream of the ridge at the location of the SH in the subset of years with high SH activity. A further finding is a distinctively different response north and south of about 50° N. The latter finding and the westward displacement noted above lead

to changes in the background flow for the development of cyclones over the Mediterranean. The difference in position of the main trough south of 50˚ N between the two subsets of years with high and low activity can explain the most significant result on the changes in cyclonic activity over the Mediterranean: noticeably higher prevalence of cyclones in the northern subarea (30˚-50˚ N, 0˚-30˚ E) during the high-activity years. The percentage relative difference of average frequency of occurrence in the northern subarea between the high- and low-activity years is about 68%. In addition to the structure of stationary wave, there are related factors that may be involved in making the cyclonic activity different in the two subsets. In this regard, one can refer to the changes in environmental static stability and baroclinicity, which may lead to changes in baroclinic instability characteristics (Soldatenko and Tingwell, 2013). Filling such gaps in our knowledge of detailed mechanisms leading to the changes observed in cyclonic activity would require a separate study.

Acknowledgments

The authors would like to thank Dr. S. Sabetghadam for her useful comments and interesting discussions. We also acknowledge Dr. M. Amiramjadi and Mr. N. Mohammadi for their help in programming with python and making the figures.

References

Ahmadi-Hojat, M., and Ahmadi-Givi, F., 2012. Examination of dynamical and thermodynamical structures of the Siberian high pressure and its amplification during the period of 1948–2008. Iranian Journal of Geophysics., 7, 107–127.

Ahrens, C. D., and Henson, R., 2018. Meteorology Today: An Introduction to Weather, Climate, and the Environment. Twelfth Edition, Cengage Learning, Boston (678 pp).

Alizadeh, Z., Mohebalhojeh, A. R., Ahmadi-Givi, F., Mirzaei, M., and Khansalari, S., 2020. The climatological impact of the upper-tropospheric Rossby wave propagation on the Red Sea trough in winter. Atmos. Res. https://doi.org/10.1016/j.atmosres.2020.105368.

Almazroui, M., Awad, A. M., Islam, M. N., and Al-Khalaf, A. K., 2015. A climatological study: wet season cyclone tracks in the East Mediterranean region. Theor. Appl. Climatol., 120, 351–365.

Almazroui, M., and Awad, A. M., 2016. Synoptic regimes associated with the eastern Mediterranean wet season cyclone tracks. Atmos. Res., 180, 92–118.

Almazroui, M., Awad, A. M., and Islam, N. M., 2017. Characteristics of the internal and external sources of the Mediterranean synoptic cyclones for the period 1956–2013. Theor. Appl. Climatol., 133, 811–827.

Aminikhanghahi, S., and Cook, D. J., 2017. A survey of methods for time series changes point detection. Knowl. Inf. Syst., 51, 339–367.

Campins, J., Genoves, A., Picornell, M. A., and Jansa, A., 2010. Climatology of Mediterranean cyclones using the ERA-40 dataset. Int. J. Climatol., 31, 1596–1614.

Cohen, J., Saito, K., and Entekhabi, D., 2001. The role of the Siberian high on the Northern Hemisphere climate variability. Geophys. Res. Lett., 28, 299–302.

Cohen, J., Barlow, M., Kushner, P. J., and Saito, K., 2007. Stratosphere–troposphere coupling and links with Eurasian land surface variability. J. Clim., 20 (21), 5335–5343.

Comiso, J. C., Parkinson, C. L., Gersten, R., and Stock, L., 2008. Accelerated

decline in the Arctic Sea ice cover. Geophys. Res. Lett., 35, L01703, doi:10.1029/2007GL031972.

D'Arrigo, R., Jacoby, G., Wilson, R., and Panagiotopoulos, F., 2005. A reconstructed Siberian High index since A. D. 1599 from Eurasian and North American tree rings. Geophys. Res. Lett., 32, L0570, doi: 10.1029/2004GL022271.

Dayan, U., Nissen, K., and Ulbrich, U., 2015. Atmospheric conditions inducing extreme precipitation over the eastern and western Mediterranean. Nat. Hazards Earth Syst. Sci., 15, 2525–2544.

Ding, Y., 1990. Build-up, air mass transformation and propagation of Siberian high and its relation to cold surge in East Asia. Meteoro. Atmos. Phys., 44, 281–292.

Ding, Y., and Krishnamurti, T. N., 1987. Heat budget of the Siberian high and winter monsoon. Mon. Wea. Rev., 115, 2428–2449.

Eshel, G., and Farrell, B. F., 2000. Mechanisms of eastern Mediterranean rainfall variability. J. Atmos. Sci., 57, 3219–3232.

Eshel, G., Cane, M. A., and Farrell, B. F., 2000. Forecasting eastern Mediterranean droughts. Mon. Wea. Rev., 128, 3618–3630.

Fei, L., and Yong-Qi, G., 2015. The project Siberian High in CMIP5 models. Atmos. Ocea. Sci. Lett., 4, 179–184.

Flaounas, E., Kotroni, V., Lagouvardos, K., Gray, S. L., Rysman, J-F., and Claud, C., 2018. Heavy rainfall in Mediterranean cyclones. Part I: contribution of deep convection and warm conveyor belt. Clim. Dynam., 50, 2935–2949. doi: 10.1007/s00382-017-3783-x.

Flaounas, E., Davolio, S., Raveh-Rubin, S., Pantillon, F., Miglietta, M. M., Gaertner, M. A., Hatzaki, M., Homar, V., Khodaya, S., Korres, G., Kotroni, V., Kushta, J., Reale, M., and Ricard, D., 2022. Mediterranean cyclones: current knowledge and open questions on dynamics, prediction, climatology and impacts. Weather and Clim. Dynam., 3, 173–208. https://doi.org/10.5194/wcd-3-173-2022.

Flocas, H. A., Simmonds, I., Kouroutzoglou, L., Keay, K., Hatzaki, M., Bricolas, V., and Asimakopoulos, D., 2010. On cyclonic tracks over the Eastern Mediterranean. J. Clim., 23, 5243–5257. doi: 10.1175/2010JCLI3426.1.

Gong, D. Y., and Ho, C. H., 2002. The Siberian High and climate change over middle to high latitude Asia. Theor. Appl. Climatol., 72, 1–9.

Haggag, M., and El-Badry, H., 2013. Mesoscale numerical study of quasi-stationary convective system over Jeddah in November 2009. Atmos. Clim. Sci., 3(1), 73–86.

Hasanean, H. M., Almazroui, M., Jones, P. D., and Alamoudi, A. A., 2013. Siberian high variability and its teleconnections with tropical circulations and surface air temperature over Saudi Arabia. Clim. Dyn., 41, 2003–2018.

Held, I. M., Ting, M., and Wang, H., 2002. Northern winter stationary waves: Theory and modeling. J. Clim., 15, 2125–2144.

Jeong, J. H., Ou, T., Linderholm, H. W., et al., 2011. Recent recovery of the Siberian High intensity. J. Geophys. Res., 116, D23102, doi:10.1029/2011JD015904.

Kobayashi, S., Ota, Y., Harada, Y., Ebita, A., Moriya, M., Onoda, H., Onogi, K., Kamahori, H., Kobayashi, C., Endo, H., Miyaoka, K., and Takahashi, K., 2015. The JRA-55 reanalysis: General specifications and basic characteristics. J. Meteor. Soc. Japan, 93, 5–48.

Labban, A. H., Mashat, A. W. S., and Awad, A. M., 2020. The variability of

the Siberian high ridge over the Middle East. Int. J. Climatol., doi: 10.1002/joc.6611.

Lionello, P., Trigo, I. F., Gil, V., Liberato, M. L. R., Nissen, K. M., Pinto, J. G., Raible, C. C., Reale, M., Tanzarell, A., Trigo, R. M., Ulbrich, S., and Ulbrich, U., 2016. Objective climatology of cyclones in the Mediterranean region: a consensus view among methods with different system identification and tracking criteria. Tellus A: Dynamic Meteorology and Oceanography, 68:1, 29391, DOI: 10.3402/tellusa.v68.29391.

Lydolf, P. E., 1977. Climates of the Soviet Union. Elsevier (443 pp).

Maheras, P., Flocas, H., Patrikas, I., and Anagnostopoulou, C., 2001. A 40-year objective climatology of surface cyclones in the Mediterranean region: spatial and temporal distribution. Int. J. Climatol., 21(1), 109–130.

Nasr-Esfahany, M. A., Ahmadi-Givi, F., and Mohebalhojeh, A. R., 2011. An energetic view of the relation between the Mediterranean storm track and the North Atlantic Oscillation. Quart. J. R. Meteorol. Soc. 137, 749 – 756.

Panagiotopoulos, F., Shahgedanova, M., Hannachi, A., and Stephenson, D. B., 2005. Observed trends and teleconnections of the Siberian high: a recently declining center of action. J. Clim., 18, 1411–1422.

Petterssen, S., 1956. Weather Analysis and Forecasting. Volume I., McGraw-Hill (266 pp).

Reale, M., Narvaez, W. D. C., Cavicchia, L., Conte, D., Coppola, E., Flaounas, E., Giorgi, F., Guald, S., Hochman, A., Li, L., Lionello, P., Podrascanin, Z., Salon, S., Sanchez-Gomez, E., Scoccimarro, E., Sein, D. V., and Somot, S., 2022. Future projections of Mediterraneancyclone characteristicsusing the Med-CORDEXensemble of coupled regional climate system models. Clim. Dynam., 58, 2501–2524.

Rezaeian, M., Moheballhojeh, A. R., Ahmadi-Givi, F., and Nasr-Esfahany, M. A., 2016. A wave- activity view of the relation between the Mediterranean storm track and North Atlantic Oscillation in winter. Quart. J. R. Meteorol. Soc., 144, 2–20.

Rodionov, S. N., 2004. A sequential algorithm for testing climate regime shifts. Geo. Res. Lett., 31, L0924, doi:10.1029/2004GL019448.

Rodwell, M. J., Rowell, D. P., and Folland, C. K., 1999. Oceanic forcing of the wintertime North Atlantic Oscillation and European climate. Nature, 398, 320–323.

Rogers, J. C., 1997. North Atlantic storm track variability and its association to the North Atlantic Oscillation and climate variability of northern Europe. J. Clim., 10, 1635–1647.

Sahsamanglou, H. S., Makrogiannis, T. J., and Kallimopoulos, P. P., 1991. Some aspects of the basic characteristics of the Siberian anticyclone. Int. J. Climatol., 11, 839–827.

Soldatenko, S., and Tingwell, C., 2013. The sensitivity of characteristics of large scale baroclinic unstable waves in Southern Hemisphere to the underlying climate. Advances in Meteorology, Aticle ID 981271, 11 pp, http://dx.doi.org/10.1155/2013/981271

Takaya, K., and Nakamura, H., 2005, Mechanism of interseasonal amplification of the cold Siberian high. J. Atmos. Sci., 62, 4423–4440.

Thorncroft, C. D., Hoskins, B. J. and McIntyre, M. E., 1993. Two paradigms of baroclinic-wave life-cycle behavior. Quart. J. R. Meteorol. Soc., 119, 17–55.

Trigo, I. F., Davies, T. D., and Bigg, G. R., 1999. Objective climatology of cyclones in the Mediterranean region. J. Clim., 12(6), 1685–1696.

Trigo, I. F., Bigg, G. R., and Davies, T. D., 2002. Climatology of cyclogenesis mechanisms in the Mediterranean. Mon Wea. Rev., 130, 549-569.

Tubi, A., and Dayan, U., 2013. The Siberian High: teleconnections, extremes and association with the Icelandic Low. Int. J. Climatol., 33(6), 1357–1366.

Wallace, J. M., 1983. The climatological mean stationary waves: Observational evidence. Large-Scale Dynamical Processes in the Atmosphere, B. J. Hoskins and R. P. Pearce, Eds., Academic Press, 27–53.

Wernli, H., and Schwierz, C., 2006. Surface cyclones in the ERA-40 dataset (1958 – 2001). Part I: novel identification method and global climatology. J Atmos. Sci., 63(10), 2486–2507.

Zhao, S., Feng, T., Tie, X., Long, X., Li, G., Cao, J., Zhou, W., and An, Z., 2018. Impact of climate change on Siberian High and wintertime air pollution in China in past two decades. Ear. Fut., 6, 118–133.